Impact of Noncovalent Sulfur–Fluorine Interaction Position on Properties, Structures, and Photovoltaic Performance in Naphthobisthiadiazole-Based Semiconducting Polymers

Masahiko Saito, Tomohiro Fukuhara, Satoshi Kamimura, Hiroyuki Ichikawa, Hiroyuki Yoshida, Tomoyuki Koganezawa, Yutaka Ie,* Yasunari Tamai, Hyung Do Kim, Hideo Ohkita,* and Itaru Osaka*

Controlling the energetics and backbone order of semiconducting polymers is essential for the performance improvement of polymer-based solar cells. The use of fluorine as the substituent for the backbone is known to effectively deepen the molecular orbital energy levels and coplanarize the backbone by noncovalent interactions with sulfur of the thiophene ring. In this work, novel semiconducting polymers are designed and synthesized based on difluoronaphthobisthiadiazole (FNTz) as a new family of naphthobisthiadiazole (NTz)–quaterthiophene copolymer systems, which are one of the highest performing polymers in solar cells. The effect of the fluorination position on the energetics and backbone order is systematically studied. It is found that the dependence of the solar cell fill factor on the active layer thickness is very sensitive to the fluorination position. It is thus further investigated and discussed how the structural features of the polymers influence the photovoltaic parameters as well as the diode characteristics and bimolecular recombination. Further, the polymer with fluorine on both the naphthobisthiadiazole and quaterthiophene moieties exhibits a quite high power conversion efficiency of 10.8% in solar cells in combination with a fullerene. It is believed that the results would offer new insights into the development of semiconducting polymers.

1. Introduction

Semiconducting polymers are an important class of functional materials that can be solution-processed to form thin films on plastic substrates and thus can be applied to various flexible optoelectronic devices.[1–3] One of the devices that are most strongly reliant on the properties of semiconducting polymers is organic photovoltaics (OPVs), in which the semiconducting polymers are typically used as the p-type (electron donor) material in combination with fullerene derivatives or nonfullerene small molecules as the n-type (electron acceptor) material.[4–12] Research of OPVs has seen great advances in the last decade owing to the development of a wide variety of semiconducting polymers with donor–acceptor motifs wherein electron-rich and electron-deficient π-conjugated building units (donor and acceptor) are alternately incorporated in the backbone.[13–22] This design strategy has enabled us to easily tune polymer

Dr. M. Saito, S. Kamimura, Prof. I. Osaka
Department of Applied Chemistry
Graduate School of Engineering
Hiroshima University
1-4-1 Kagamiyama, Higashi-Hiroshima, Hiroshima 739-8527, Japan
E-mail: iosaka@hiroshima-u.ac.jp
T. Fukuhara, Dr. Y. Tamai, Dr. H. D. Kim, Prof. H. Ohkita
Department of Polymer Chemistry
Graduate School of Engineering
Kyoto University
Katsura, Nishikyo-ku, Kyoto 615-8510, Japan
E-mail: ohkita@photo.polym.kyoto-u.ac.jp

The ORCID identification number(s) for the author(s) of this article can be found under https://doi.org/10.1002/aenm.201903278.

H. Ichikawa, Prof. H. Yoshida
Department of Materials Science
Graduate School of Engineering
Chiba University
1-33 Yayoi-cho Inage-ku, Chiba 263-8522, Japan
Prof. H. Yoshida
Molecular Chirality Research Center
Chiba University
1-33 Yayoi-cho Inage-ku, Chiba 263-8522, Japan
Dr. T. Koganezawa
Japan Synchrotron Radiation Research Institute (JASRI)
1-1-1 Kouto, Sayo-cho, Sayo-gun, Hyogo 679-5198, Japan
Prof. Y. Ie
The Institute of Scientific and Industrial Research (ISIR)
Osaka University
8-1 Mihogaoka, Ibaraki, Osaka 567-0047, Japan
E-mail: yutakaie@sanken.osaka-u.ac.jp
Dr. Y. Tamai
PRESTO
Japan Science and Technology Agency (JST)
4-1-8 Honcho, Kawaguchi, Saitama 332-0012, Japan

**ADVANCED
SCIENCE NEWS**

www.advancedsciencenews.com

**ADVANCED
ENERGY
MATERIALS**

www.advenergymat.de

properties. Recent studies of nonfullerene n-type materials have further enhanced the performance of OPVs.[8,12,23–26] In addition, semiconducting polymers as the n-type material have also been intensively studied.[27–35]

The requirements for semiconducting polymers to improve the power conversion efficiency (PCE) with respect to the electronic properties include a narrow optical bandgap (E_g) and a deep highest occupied molecular orbital (HOMO) energy level, which in principle would maximize the short-circuit current density (J_{SC}) and the open-circuit voltage (V_{OC}), respectively.[36] Further, the lowest unoccupied molecular orbital (LUMO) energy level is also important because the offset energy of the LUMOs between the p- and n-type materials, particularly when the p-type material has a narrower bandgap than the n-type material, would dictate the photon energy loss (E_{loss}), which is calculated by $E_g - eV_{OC}$, where e is the elementary charge.[37–39] Thus, the LUMO energy level of the p-type material should be deep and as close as that of the n-type material, which would diminish the offset energy and thereby increase V_{OC}. In the meantime, the desired structural features for the semiconducting polymers are high crystallinity and backbone orientation with the "face-on" motif.[40–43] Such favorable structural features would bring about high charge carrier mobility, which is crucial for a high fill factor (FF). It would also enable the use of thick active layers, which are beneficial for increasing light absorption and thus J_{SC}.[44,45]

The incorporation of large π-conjugated building units with strong electron deficiency is an effective way to ensure the coplanarity of the polymer backbone and thereby a high crystallinity as well as deep energy levels.[13,14,16,20–22] On the other hand, the introduction of substituents with an electron-withdrawing nature that realizes noncovalent intramolecular interactions also brings about these electronic and structural features.[46] The fluorine atom is one of the most widely used substituents for this purpose in semiconducting polymers because it has the highest electronegativity among all the elements and shows attractive interaction with hydrogen and sulfur atoms.[47–49] However, the position and the number of substituents largely affect the electronic properties, the ordering structures, and the solubility of the polymers. Therefore, the implications of such substituents have to be carefully examined to design semiconducting polymers with even higher performance.

One good example is a series of semiconducting polymers consisting of a naphtho[1,2-*c*:5,6-*c*′]-bis[1,2,5]thiadiazole (NTz)[7,9,20,50–52] strongly electron deficient building unit (**Figure 1**a) and a quaterthiophene moiety with two long branched alkyl groups. We reported that an NTz-based polymer, **PNTz4T** (Figure 1a), showed crystalline structures with the face-on orientation in the polymer/fullerene blend film, which led to PCEs of ≈10% in the PC₇₁BM-based cell.[9] More recently, we developed fluorinated NTz-based polymers, **PNTz4TF2** and **PNTz4TF4** (Figure 1b), in which two and four fluorine atoms were introduced into the β-positions of the bithiophene moiety, respectively (Figure 1b).[50] Both fluorinated polymers had deeper HOMO energy levels than **PNTz4T**, whereas they had wider optical bandgaps than **PNTz4T**. Further, as the fluorine number increased, the backbone coplanarity was apparently enhanced but the fraction of the face-on orientation was

decreased in the blend film: in particular, **PNTz4TF4** oriented rather randomly. Overall, the **PNTz4TF2** cell exhibited as high as 10.5% PCE, whereas the **PNTz4TF4** cell exhibited a limited PCE of ≈6.5%.

Very recently, Ie and co-workers reported the synthesis of difluorinated NTz (FNTz) (Figure 1a) as well as an FNTz-based small molecule that nicely functioned as an n-type material in an OPV cell.[53] FNTz would thus allow us to examine the effect of fluorination on the NTz moiety in the **PNTz4T** backbone. Here, we synthesized for the first time FNTz-based semiconducting polymers, **PFN4T** and **PFN4TF2** (Figure 1c), as new members of the **PNTz4T** family. Furthermore, we systematically studied the effect of the fluorine substitution position on the polymer electronic structure, the ordering structure, and the photovoltaic properties by comparing with counterpart polymers **PNTz4T** and **PNTz4TF2**. **PFN4TF2**, which has two fluorine atoms each on the NTz moiety and the bithiophene moiety, showed as high as 10.8% PCE and reduced E_{loss} in PC₇₁BM-based OPV cells. To better distinguish the chemical structure, we renamed the polymers as **Fn–Fn**, where the first and the second "F" represent fluorine at the NTz moiety and the bithiophene moiety, respectively, and "*n*" represents the number of substituted fluorine atoms in each moiety. Thus, **PNTz4T**, **PNTz4TF2**, **PNTz4TF4**, **PFN4T**, and **PFN4TF2** will be hereinafter called **F0–F0**, **F0–F2**, **F0–F4**, **F2–F0**, and **F2–F2**, respectively (Figure 1a–c).

2. Synthesis of Polymers

The synthetic route to the FNTz-based polymers is displayed in Figure 1d. FNTz, synthesized according to a previous report,[53] was first brominated by *N*-bromosuccinimide (NBS) to give **1**, and **1** was reacted with stannylated alkylthiophenes (**2a**: R = 2-decyltetradecyl (DT), **2b**: R = 2-dodecylhexadecyl (DH)) via the Stille coupling reaction to afford **3a** and **3b**, respectively. Then, **3a** and **3b** were dibrominated by NBS to provide **4a** and **4b**, respectively, as the monomers for polymerization. **4a** and **4b** were copolymerized with distannylated bithiophene (**5a**) and distannylated difluorobithiophene (**5b**), respectively, via the Stille coupling reaction under microwave irradiation to afford **F2–F0** and **F2–F2**.

The polymers were soluble in hot chlorinated solvents, such as chlorobenzene (CB) and *o*-dichlorobenzene (DCB). Whereas the DT group was introduced as the side chain of **F2–F0**, the DH group, which is longer than the DT group, was introduced to **F2–F2**. This is because **F2–F2** with four fluorine atoms showed reduced solubility and **F2–F2** having the DT group as the side chain was barely soluble in the above conditions. Number-average and weight-average molecular weights (M_n and M_w) determined by high-temperature gel-permeation chromatography (GPC) were 33.5 and 79.1 kDa with a polydispersity index (PDI) of 2.3 and 66.3 and 529 kDa with a PDI of 8.0 for **F2–F0** and **F2–F2**, respectively (Table S1, Supporting Information). The large PDI for **F2–F2** is due to the broad GPC peak that probably originated in the strong aggregation property (Figure S1, Supporting Information).[54–56] The thermal properties of the polymers were investigated by differential scanning calorimetry
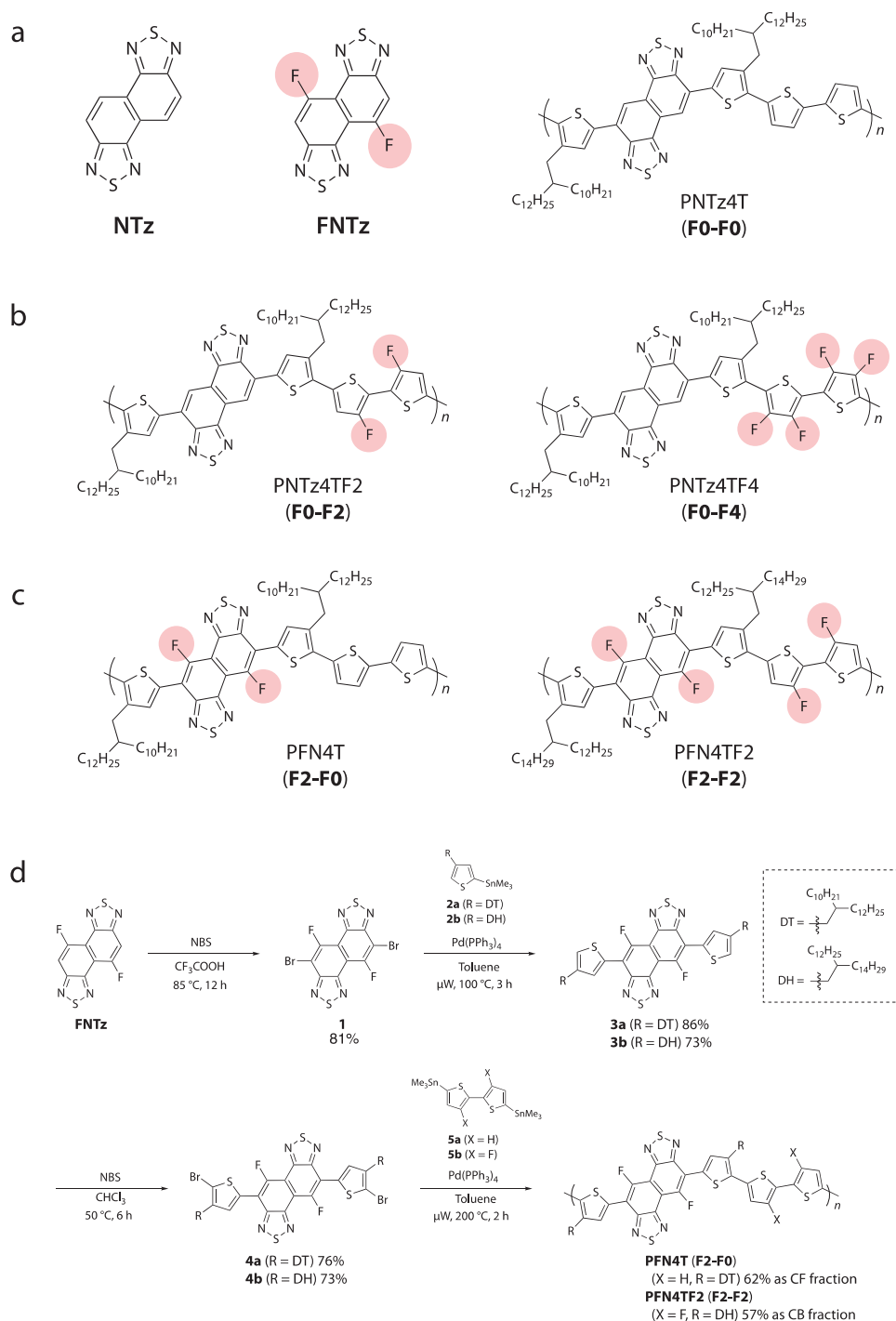
1903278 (2 of 12)

Figure 1. a) Chemical structures of **NTz** and **FNTz**, and **PNTz4T** (**F0–F0**). b) Derivatives of **F0–F0** with fluorine atoms on the bithiophene moiety, **PNTz4TF2** (**F0–F2**) and **PNTz4TF4** (**F0–F4**). c) FNTz-based polymers: **PFN4T** (**F2–F0**) and **PFN4TF2** (**F2–F2**). d) Synthetic route to **F2–F0** and **F2–F2**.

(DSC). Whereas **F2–F0** showed a melting peak at 340 °C, **F2–F2** did not show any peak below 350 °C (Figure S2, Supporting Information). This indicates that both polymers do not undergo phase transitions under the conditions for cell fabrication and measurements. The properties of **F0–F0** and **F0–F2** used in this study are also summarized in Table S1 (Supporting Information).

3. Influence of Fluorination Position on Electronic and Optical Properties, and Backbone Order

The HOMO and LUMO energy levels (E_H and E_L) of the polymers were examined by photoelectron yield spectroscopy (PYS) (**Figure 2**a) and low-energy inverse photoelectron spectroscopy (LEIPS)[57,58] (Figure 2b) using the polymer thin films, and
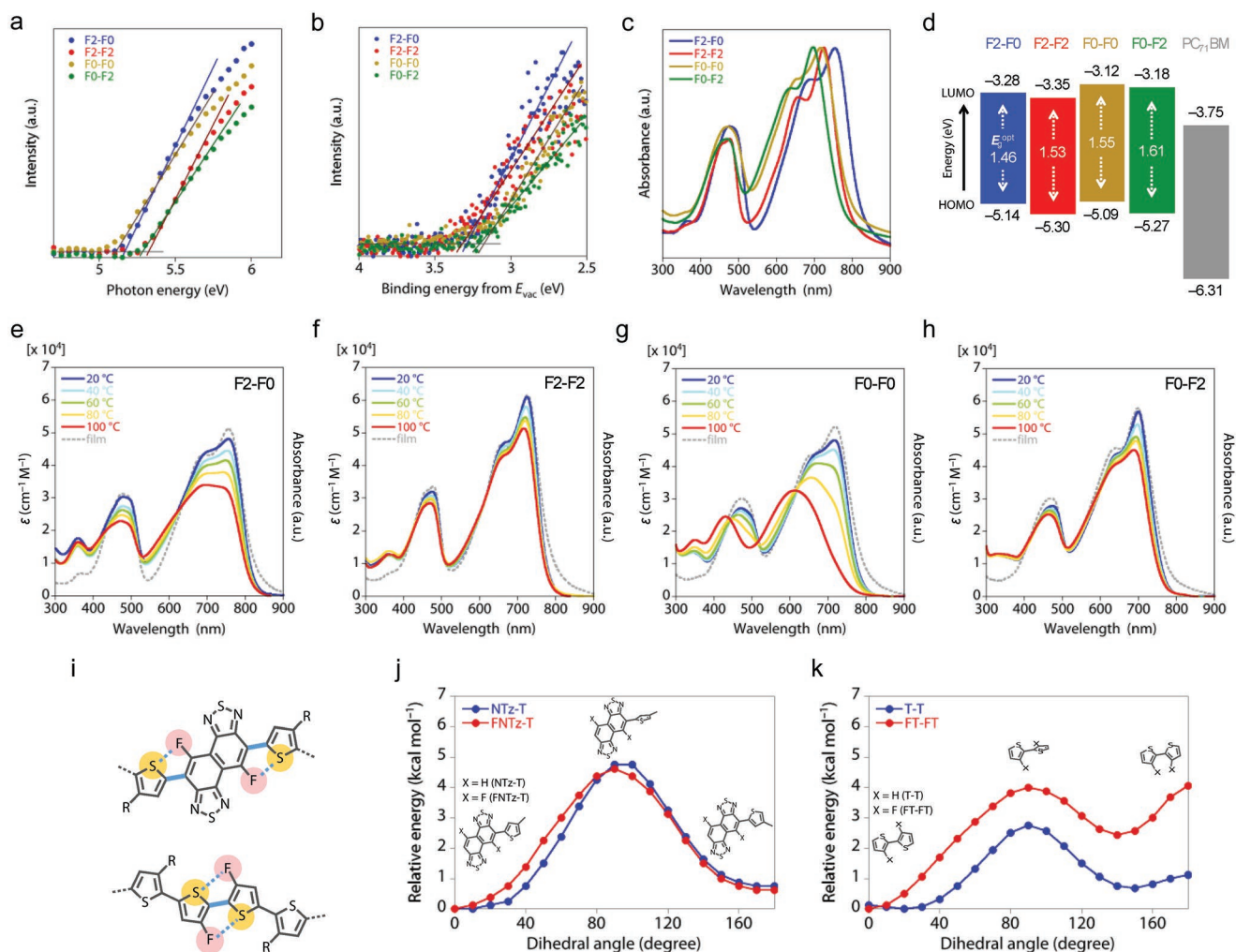
Figure 2. a) Photoelectron yield spectra (PYS) of the polymers. b) Low-energy inverse photoelectron spectra (LEIPS) of the polymers. c) UV–vis absorption spectra of the polymers in the thin films. d) Energy diagrams of the polymers and $PC_{71}BM$. HOMO and LUMO energy levels determined by PYS and LEIPS are used. e–h) Temperature-dependent UV–vis absorption spectra of the polymers in CB solution: e) **F2–F0**, f) **F2–F2**, g) **F0–F0**, and h) **F0–F2**. i) Noncovalent F···S interactions at the FNTz–alkylthiophene bonds (upper) and the thiophene–thiophene bond (lower). j,k) Energy variation of the model compounds (NTz-T, FNTz-T, T-T, and FT-FT) as a function of the rotation angle determined by the DFT method at the B3LYP/6-31d g) level for j) NTz-T and FNTz-T, and k) T-T and FT-FT.

are summarized in Figure 2d and Table 2. **F2–F0** had an E_H of −5.14 eV, which was slightly deeper by 0.05 eV than that of **F0–F0**. However, it had an E_L of −3.28 eV, which was deeper by 0.16 eV than that of **F0–F0**. This indicates that the fluorination on the NTz moiety affected LUMO more than HOMO. This is fairly consistent with the fact that the LUMOs mainly reside on the NTz moiety according to the computation carried out by the DFT method (B3LYP/6-31g(d)) (Figure S4, Supporting Information). When **F2–F2** was compared with **F0–F2**, the downward shift of E_L was also larger than that of E_H: E_H and E_L of **F2–F2** were −5.30 and −3.35 eV, respectively, and those of **F0–F2** were −5.27 and −3.18 eV, respectively. However, these results contrasted with the results when the fluorine atoms were introduced onto the bithiophene moiety. When **F2–F2** was compared with **F2–F0**, whereas E_H of **F2–F2** was downshifted by 0.16 eV, E_L was downshifted by only 0.07 eV. This was consistent with the comparison between **F0–F0** and **F0–F2**, and also with the

computation in which the HOMOs mainly resided on the bithiophene moiety (Figure S4, Supporting Information). The energy levels measured by PYS and LEIPS were likely affected by the orientation of the polymer backbone.[59,60] Thus, although the energy levels determined here could be well explained by the electronic effect of the fluorine atom, these values might include some effect from orientation because the backbone orientation of these polymers was altered by the fluorination, as will be discussed later. In addition, cyclic voltammetry (CV) was also carried out to investigate E_H and E_L of the polymers (Figure S5, Supporting Information). E_H and E_L that were calculated using the redox potentials that were determined at the onset of the peaks are summarized in **Table 1**. Although the values were somewhat different from those determined by PYS and LEIPS, the trend showed good agreement.

Figure 2c displays the UV–vis absorption spectra of the polymers in the thin films. The absorption maximum (λ_{max}),

Table 1. Optical and electrochemical properties of the polymer thin films.

Polymer	E_H [eV][a]		E_L [eV][b]		λ_{max} [nm][c]	λ_{edge} [nm][d]	E_g^{opt} [eV][e]
	PYS	CV	LEIPS	CV			
F2–F0	−5.14	−5.25	−3.28	−3.55	760	850	1.46
F2–F2	−5.30	−5.48	−3.35	−3.60	727	810	1.53
F0–F0	−5.09	−5.20	−3.12	−3.46	716	798	1.55
F0–F2	−5.27	−5.42	−3.18	−3.49	694	770	1.61

[a]HOMO energy levels determined by photoelectron yield spectroscopy (PYS) and cyclic voltammetry (CV); [b]LUMO energy levels determined by low-energy photoelectron spectroscopy (LEIPS) and CV; [c]Absorption maximum; [d]Absorption edge; [e]Optical bandgap determined from the absorption edge.

the absorption edge (λ_{edge}), and the optical bandgap (E_g^{opt}) calculated using λ_{edge} are summarized in Table 1 (The E_g^{opt}s are also shown in Figure 2d). All the polymers gave a spectrum with the main band spanning ≈500–800 nm, in which two peaks were observed: in **F2–F0** and **F0–F0**, the peak in the shorter wavelength region appeared as a shoulder. The peaks were assigned to the 0–0 (700–760 nm) and 0–1 (620–700 nm) vibrational bands. The intensity ratio of the 0–0 to 0–1 bands was larger in **F2–F2** and **F0–F2** than **F2–F0** and **F0–F0**, implying that the polymers with fluorine on the bithiophene moiety are more ordered than the polymers with unsubstituted bithiophene. This will be further discussed later. λ_{max} and λ_{edge} of **F2–F0** were 760 and 850 nm, respectively, both of which were red-shifted by ≈50 nm from those of **F0–F0** (λ_{max} = 716 nm, λ_{edge} = 798 nm). Accordingly, E_g^{opt} of **F2–F0** was calculated to be 1.46 eV, which was reduced by ≈0.1 eV relative to that of **F0–F0** (E_g^{opt} = 1.55 eV). As the first excitation is dominated by the electron transition from HOMO to LUMO, the observed shifts in the absorption spectra are consistent with the effects of the fluorine substitution discussed above. Similarly, **F2–F2** also gave an absorption band (λ_{max} = 727 nm, λ_{edge} = 810 nm) that was red-shifted from that of **F0–F2** (λ_{max} = 694 nm, λ_{edge} = 770 nm) by ≈40 nm, resulting in an E_g^{opt} of 1.53 eV that was reduced by ≈0.1 eV relative to that of **F0–F2**. Thus, it is concluded that the fluorination on the NTz moiety can reduce the bandgap of the polymer. This sharply contrasts the fluorination on the bithiophene moiety that enlarges E_g^{opt} of 1.46 eV for **F2–F0** to 1.53 eV for **F2–F2**.

We also measured the UV–vis absorption spectra of the polymers in CB solution by changing the temperature (Figure 2e–h). At room temperature, all the polymers gave a main broad absorption at around 500–800 nm, in which the 0–0 and 0–1 bands were observed, similarly to the film spectrum. Such similarity likely means that the polymer backbones are partially aggregated even in solution. However, these two bands had less features in solution than in film for **F2–F0** and **F0–F0** suggesting that their backbones are less aggregated than the **F2–F2** and **F0–F2** backbones. The shapes of the room temperature spectra for **F2–F0** and **F2–F2** are very similar to those for **F0–F0** and **F0–F2**, respectively, although the peak locations are different. This suggests that the fluorination on the NTz moiety does not affect the coplanarity of the backbone. In **F2–F0** (Figure 2e), when the temperature was gradually increased to 100 °C, the spectrum became almost featureless and slightly broadened toward the shorter wavelength region, which implies that disaggregation occurred and the motion of the backbone became

large. Such behavior was more significant in **F0–F0** (Figure 2g), where its spectrum became a single broad spectrum and largely blue-shifted. This suggests that the **F2–F0** backbone is more rigid than the **F0–F0** backbone, most likely due to the noncovalent F⋯S interactions between the FNTz moiety and the neighboring alkylthiophene moiety, although the coplanarity is similar at room temperature, as mentioned above. In contrast, **F2–F2** did not show such behavior (Figure 2f). In **F2–F2**, the intensity ratio of the 0–0 band to the 0–1 band slightly decreased by raising the temperature, which implies that disaggregation and/or motion of the backbone was very limited and thus the **F2–F2** backbone was more rigid than the **F2–F0** backbone. This would originate in the additional noncovalent F⋯S interactions in the bithiophene moiety. **F0–F2** showed similar temperature-dependent spectra to **F2–F2** (Figure 2h). However, if the sizes of the alkyl side chains were the same for **F0–F2** and **F2–F2**, the behavior would be different, such as the case in **F2–F0** and **F0–F0**. It is also important to carefully compare the difference between **F0–F0** and **F2–F0**, and between **F0–F0** and **F0–F2**. Although the number of fluorine atoms is two for both **F2–F0** and **F0–F2**, the backbone rigidity was larger in **F0–F2** than **F2–F0**. This clearly demonstrates that fluorination on the bithiophene moiety results in more significant intramolecular locking than that on the NTz moiety.

The difference in the fluorination effect on the backbone rigidity can be explained as follows. On the one hand, in **F2–F0**, there are two locking sites both bonding FNTz and neighboring alkylthiophene, and there is one noncovalent F⋯S interaction at each site (Figure 2i, upper). On the other hand, in **F0–F2**, there is only one locking site bonding two fluorothiophenes, but there are two F⋯S interactions at this site (Figure 2i, lower). Therefore, it is concluded that although both polymers have two F⋯S interactions in total, the locking effect is stronger when one bond is locked by two interactions than when two bonds are each locked by one interaction. This is further supported by the computation of model compounds: NTz-thiophene (NTz-T), FNTz-thiophene (FNTz-T), bithiophene (T-T), and difluorobithiophene (FT-FT). More specifically, we calculated the total energy of the compounds with different dihedral angles and plotted the energy variation relative to the energy at the dihedral angle of 0° as a function of the dihedral angle (Figure 2j,k). The energy barrier for twisting the chemical bond for NTz-T and FNTz-T was very similar, whereas that for FT-FT was approximately twice as high as that for T-T. In addition, the optimized backbone structure is more coplanar in **F2–F2** and **F0–F2** than **F2–F0** and
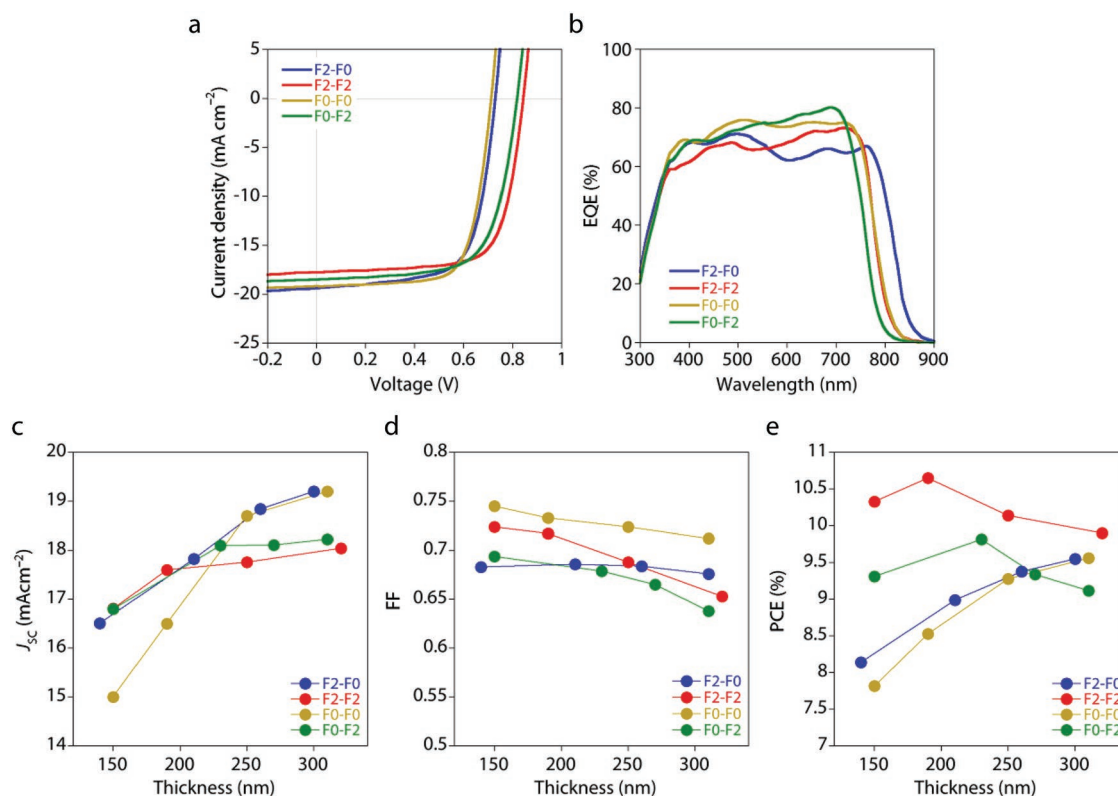
**ADVANCED
SCIENCE NEWS**
www.advancedsciencenews.com

**ADVANCED
ENERGY
MATERIALS**
www.advenergymat.de

Figure 3. a) J–V curves and b) EQE spectra of the optimized polymer/PC$_{71}$BM cells. Thickness dependence of c) J_{SC}, d) FF, and e) PCE of the cells.

F0–F0 (Figure S4, Supporting Information), which would also support this explanation.

4. Photovoltaic Properties

We fabricated OPV cells with ITO/ZnO/photoactive layer/MoO$_x$/Ag stacking. The photoactive layer was composed of the polymer and PC$_{71}$BM. The optimum polymer to PC$_{71}$BM weight ratio was 1:1.5 for the **F2–F2** cell and 1:2 for the other cells. The current density (J)–voltage (V) curves and the external quantum efficiency (EQE) spectra of the optimized cells are displayed in **Figure 3**a,b, respectively, and the photovoltaic parameters are summarized in **Table 2**. Here, we compared the photovoltaic parameters between the cells based on NTz polymers and those based on FNTz polymers. As expected from the deeper E_H for the polymers based on FNTz, the **F2–F0** and **F2–F2** cells exhibited slightly higher V_{OC} values of 0.73 and

0.84 V than the **F0–F0** cell (0.71 V) and the **F0–F2** cell (0.81 V), respectively. Consequently, E_{loss} was 0.73 eV for the **F2–F0** cell and 0.69 eV for the **F2–F2** cell, which were reduced by ca. 0.1 eV from that of the **F0–F0** (0.84 eV) and **F0–F2** (0.80 eV) cells, respectively. In contrast, although **F2–F0** and **F2–F2** had a somewhat wider absorption range (narrower E_g^{opt}) than **F0–F0** and **F0–F2**, respectively, the short-circuit current density (J_{SC}) values of the cells that used **F2–F0** (J_{SC} = 19.2 mA cm^{-2}) and **F2–F2** (J_{SC} = 17.8 mA cm^{-2}) were slightly reduced relative to those of cells that used **F0–F0** (J_{SC} = 19.4 mA cm^{-2}) and **F0–F2** (J_{SC} = 19.3 mA cm^{-2}). This is in good agreement with the result showing that the EQE values are lower nearly throughout the absorption range for the **F2–F0** and **F2–F2** cells than the **F0–F0** and **F0–F2** cells, respectively. Nevertheless, overall PCE of the **F2–F0** cell was 9.6%, which was the same as that of the **F0–F0** cell (PCE = 9.6%), and PCE of the **F2–F2** cell was 10.8%, which was reasonably enhanced compared to that of the **F0–F2** cell (PCE = 10.1%).

Table 2. Photovoltaic parameters of the optimized polymer/PC$_{71}$BM cells.

Polymer	Thickness [nm][a]	J_{SC} [mA cm^{-2}]	V_{OC} [V]	FF	PCE [%][b]	E_{loss} [eV][c]
F2–F0	300	19.2	0.73	0.68	9.6 [9.2]	0.73
F2–F2	190	17.8	0.84	0.72	10.8 [10.4]	0.69
F0–F0	320	19.4	0.71	0.71	9.6 [9.2]	0.84
F0–F2	240	19.3	0.81	0.68	10.1 [9.7]	0.80

[a]Thickness of the active layer; [b]Maximum power conversion efficiency. In the brackets are average power conversion efficiencies obtained from more than 10 devices; [c]Photon energy loss defined by $E_g - eV_{OC}$.

**ADVANCED
SCIENCE NEWS**

www.advancedsciencenews.com

**ADVANCED
ENERGY
MATERIALS**

www.advenergymat.de

Interestingly, we found clear dependence of the photovoltaic properties on the fluorination position when the active layer thickness was changed (Figures S6 and S7, Supporting Information). Figure 3c–e depict the dependence of J_{SC}, FF, and PCE on the active layer thickness. In **F2–F0** and **F0–F0**, J_{SC} increased as the active layer thickness increased to above 300 nm, most likely due to the increased photon absorption, whereas in **F2–F2** and **F0–F2**, J_{SC} increased at first but almost plateaued at around 200 nm thickness (Figure 3c). With respect to FF, in **F2–F0** and **F0–F0**, FF decreased very gently as the thickness increased, whereas in **F2–F2** and **F0–F2**, it decreased steeply (Figure 3d). As a result, **F2–F0** and **F0–F0** showed gradual increases in PCE with increasing thickness, whereas **F2–F2** and **F0–F2** showed gradual decreases above 200 nm thickness (Figure 3e). Thus, the optimum thickness for the **F2–F0** and **F0–F0** cells was >300 nm, whereas that for the **F2–F2** and **F0–F2** cells was around 200 nm.

5. Thin-Film Structure

Grazing incidence X-ray diffraction (GIXD) measurements were performed to investigate polymer ordering in the thin films. 2D GIXD patterns of the polymer neat films fabricated on the ITO/ZnO substrate are shown in **Figure 4**. Although the 2D GIXD patterns need to be corrected because the diffraction data along the q_z axis ($q_{xy} = 0$) are not true specular scan,[61] we here show the 2D original patterns without the correction in order to better visualize the polymer order. For **F2–F0** and **F2–F2** neat films (Figure 4a,b), we observed diffractions in the small angle region along both the quasi-q_z ($\approx q_z$) and q_{xy} axes, which are assignable to the lamellar order for the edge-on and face-on orientations, respectively. Correspondingly, we observed a diffraction in the wide-angle region on both the q_z and q_{xy} axes, which is assignable to the π–π stacking order for the face-on
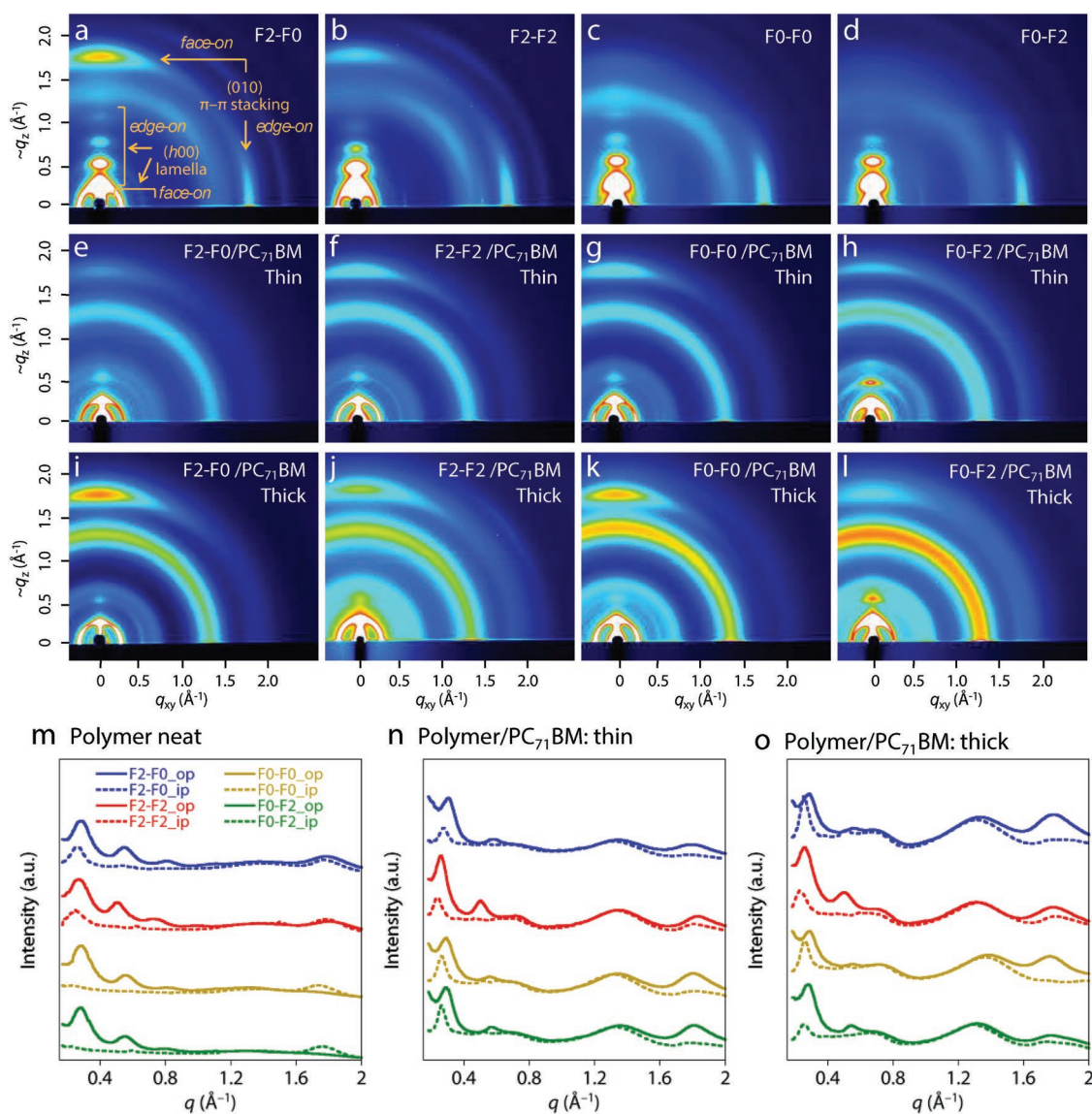

Figure 4. 2D GIXD patterns of a–d) polymer neat films, e–h) thin polymer/PC$_{71}$BM blend films, and i–l) thick blend films: a,e,i) **F2–F0**; b,f,j) **F2–F2**; c,g,k) **F0–F0**; and d,h,l) **F0–F2**. Cross-sectional diffraction profiles of m) polymer neat films, n) thin polymer/PC$_{71}$BM blend films, and o) thick blend films cut from the 2D GIXD patterns along the $\approx q_z$ axis (out-of-plane: op) (solid lines) and the $\approx q_{xy}$ axis (in-plane: ip) (dotted lines).

ADVANCED
SCIENCE NEWS
www.advancedsciencenews.com

ADVANCED
ENERGY
MATERIALS
www.advenergymat.de

and edge-on orientations, respectively.[58] It is notable that the diffraction for the face-on π–π stacking appeared more strongly in **F2–F0** than **F2–F2**. In contrast, for **F0–F0** and **F0–F2** neat films (Figure 4c,d), the lamellar and π–π diffractions were only observed along the $\approx q_z$ and q_{xy} axes, respectively, as reported previously. The results indicate that the **F2–F0** and **F2–F2** films were composed of both fractions of the edge-on and face-on orientations, whereas the **F0–F0** and **F0–F2** films were mostly dominated by the edge-on orientation. Moreover, this means that the fluorination on the NTz moiety drove the polymer backbones to lie flat on the substrate.

The cross-sectional diffraction profiles of the polymer neat films cut along the q_z and q_{xy} axes of the 2D GIXD patterns are depicted in Figure 4m, respectively. The lamellar d-spacing (d_L) of **F2–F0** and **F2–F2** in the edge-on fraction (along the q_z axis) was 22.6 Å ($q_z = 0.28$ Å^{-1}) and 24.7 Å ($q_z = 0.25$ Å^{-1}), respectively (Table S2, Supporting Information). The difference should be due to the difference of the side chain length. Interestingly, d_L of **F2–F0** was shorter than that of **F0–F0** (24.7 Å) by $\approx$2 Å, despite the fact that both polymers have the same alkyl side chain. This can be attributed to the interlocked FNTz–alkylthiophene bonds in **F2–F0**. This would afford more effective space between the adjacent side chains than nonfluorinated **F0–F0**, and thus would enable deeper side chain interdigitation, resulting in the shorter d_L. This is also the case in **F2–F2**: d_L of **F2–F2** was 24.7 Å, which was the same as that of **F0–F2** despite the fact that **F2–F2** possesses a longer side chain than **F0–F2**. Nevertheless, the d-spacing for the π–π stacking (d_π) of **F2–F0** and **F2–F2**, determined by the edge-on fraction, was 3.53 Å, which was almost the same as those of **F0–F0** and **F0–F2** (Table S2, Supporting Information).

The 2D GIXD patterns of the polymer/PC$_{71}$BM blend films were also measured. As the trend of the photovoltaic performance dependence on the active layer thickness differed by the fluorination position, we conducted measurement by using films with two different thicknesses, $\approx$100 nm (thin) (Figure 4e–h,n) and 300 nm (thick) (Figure 4i–l, o), for each polymer. In **F2–F0** and **F2–F2**, the polymer π–π stacking diffraction mainly appeared on the q_z axis, indicating that the polymers predominantly formed the face-on orientation. Both d_L and d_π of all the polymers were almost unchanged by blending with PC$_{71}$BM (**Table 3**). Although the predominant orientation in the neat films was different between the polymers with NTz and with FNTz, that in the blend films was mostly the same for

all the polymers. However, it is noted that, in **F2–F2** and **F0–F2** blend films, the polymer π–π stacking diffraction somewhat diffused as ring, suggesting that the degree of face-on orientation is relatively low and that some portions are randomly oriented. The difference in the backbone orientation was further quantified by pole figure analysis using the 2D GIXD patterns of the blend films.[9,45,62,63] The ratios of the face-on to edge-on orientation were evaluated by calculating A_f/A_e, where A_f and A_e correspond to the area of the diffraction peak for the face-on and edge-on fractions in the pole figure plots (Figure S8, Supporting Information), and are summarized in Table 3. For the thin films, A_f/A_e was higher in **F2–F0** (0.60) and **F0–F0** (0.66) than **F2–F2** (0.42) and **F0–F2** (0.26). For the thick films, although A_f/A_e was increased in all the polymers, the trend was the same as that for the thin films. These results suggest that fluorination on the bithiophene moiety deteriorates the face-on orientation in the blend film.

Polymer crystallinity was also evaluated by calculating the coherence length (L_C) by the simplified Scherrer's equation,[64,65] $L_C = 2\pi/\text{FWHM}$, where FWHM is the full width at half-maximum of the lamellar diffraction peak in the $\approx q_{xy}$ axis (face-on fraction) (Table 3). Although the L_C values evaluated here are not real values, because the FWHM values include broadening due to the instrumental resolution originating in the X-ray footprint at the sample surface, this would be a good measure to discuss the relative difference in crystallinity. Whereas all the polymers in the thin film gave similar L_C values (42–48 Å), **F2–F0** and **F0–F0** gave L_C values larger than 50 Å and **F2–F2** and **F0–F2** gave L_C values smaller than 40 Å in the thick film. The result was somewhat interesting because the polymers with the difluorinated bithiophene moiety (**F2–F2** and **F0–F2**) should have more coplanar backbones due to the noncovalent F⋯S interactions as discussed above. A plausible reason is that these polymers have relatively lower solubility due to the more coplanar backbones, which makes them solidify more quickly before self-organizing to pack in order during the spin coating, resulting in the lower crystallinity. Another possible reason is the influence of dipoles.[66] Although the dipoles are cancelled throughout the backbone due to the symmetric structure, there are certainly some local dipoles at each moiety (Figure S9, Supporting Information). Seemingly, fluorination on the bithiophene moiety changes the local dipole more significantly than on the NTz moiety. Such difference might affect the polymer crystal packing and/or orientation.

Table 3. Structural parameters of the polymers in the blend films and charge carrier mobilities of the blend films.

Polymer	d_L [Å][a)]	d_π [Å][b)]	A_f/A_e[c)]		FWHM [Å^{-1}]/L_C [Å][d)]		μ [cm^2 V^{-1} s^{-1}][e)]		
			Thin	Thick	Thin	Thick	Hole (neat)	Hole (blend)	Electron
F2–F0	22.6	3.53	0.60	1.28	0.149/42	0.108/58	2.2×10^{-3}	1.2×10^{-3}	1.3×10^{-3}
F2–F2	24.7	3.53	0.42	0.52	0.136/46	0.165/38	2.5×10^{-3}	1.1×10^{-3}	1.1×10^{-3}
F0–F0	24.7	3.55	0.66	0.90	0.131/48	0.121/52	1.6×10^{-3}	2.1×10^{-3}	1.5×10^{-3}
F0–F2	24.7	3.53	0.26	0.46	0.137/46	0.170/37	1.3×10^{-3}	0.8×10^{-3}	1.8×10^{-3}

[a)]d-Spacing corresponds to the lamellar structure of the face-on crystallite, (100) along the q_{xy} axis; [b)]d-Spacing corresponds to the π–π stacking of the face-on crystallite, (010) along the $\approx q_z$ axis; [c)]The ratio of face-on to edge-on orientation determined by pole figure analysis; [d)]FWHM and coherence length (L_C) estimated from the simplified Scherrer's equation ($L_C = 2\pi/\text{FWHM}$) for the lamellar diffraction of the face-on crystallite; [e)]Hole mobilities for the polymer-neat and polymer/PC$_{71}$BM blend films and electron mobilities for the blend films evaluated by the space-charge-limited current model.

6. Charge Carrier Mobility

The charge carrier mobility was evaluated with a hole-only device using the polymer neat film and polymer/PC$_{71}$BM blend film, and with an electron-only device using the blend film based on the space-charge-limited current (SCLC) model (Figure S10, Supporting Information and Table 3). In the polymer-neat film, the mobilities for **F2–F0** and **F2–F2** (1.3–1.6×10^{-3} cm^2 V^{-1} s^{-1}) were slightly higher than those for **F0–F0** and **F0–F2** (2.2–2.6×10^{-3} cm^2 V^{-1} s^{-1}), which is consistent with the backbone orientation. However, due to the very small difference, we regard as that these hole mobilities are basically the same. In the blend film, **F2–F0** (1.2×10^{-3} cm^2 V^{-1} s^{-1}) and **F0–F0** (2.1×10^{-3} cm^2 V^{-1} s^{-1}), having larger face-on fraction, showed higher hole mobilities than **F2–F2** (1.1×10^{-3} cm^2 V^{-1} s^{-1}) and **F0–F2** (0.8×10^{-3} cm^2 V^{-1} s^{-1}). However, the difference of the mobility was again very small, and we regard as that all the polymers have similar mobilities. Thus, it is concluded that although the GIXD studies showed that the polymers with the unsubstituted bithiophene moiety (**F2–F0** and **F0–F0**) had larger fraction of the face-on orientation and higher crystallinity than the polymers with the difluorinated bithiophene moiety (**F2–F2** and **F0–F2**), the mobility determined by the SCLC model was insensitive to such difference. The electron mobilities were also similar in all the blend films, which is quite reasonable considering that the major electron carrier is PC$_{71}$BM.

7. Charge Recombination Dynamics

Charge recombination is an important factor that determines the photovoltaic performance: suppressed charge recombination leads to efficient charge collection and hence high FFs.[67] In this section, in order to discuss how the fluorination position and the resulting polymer order affect the charge recombination in these polymers, we studied charge recombination dynamics by measuring transient photovoltage/transient photocurrent (TPV/TPC) of these solar cells with a thin or thick active layer (Figures S11–S13, Supporting Information).[68,69]

Figure 5a displays the dependence of charge carrier lifetime (τ_n) on charge carrier density (n) for the thin devices. On the basis of these values, the bimolecular recombination rate constant (k_{rec}) is given by $k_{rec} = 1/\tau_n n$. The bimolecular recombination reduction factor (ζ) is given by the ratio of k_{rec} to diffusion-limited Langevin recombination rate constant (k_L), $\zeta = k_{rec}/k_L$, which has been widely employed as a measure of how charge recombination
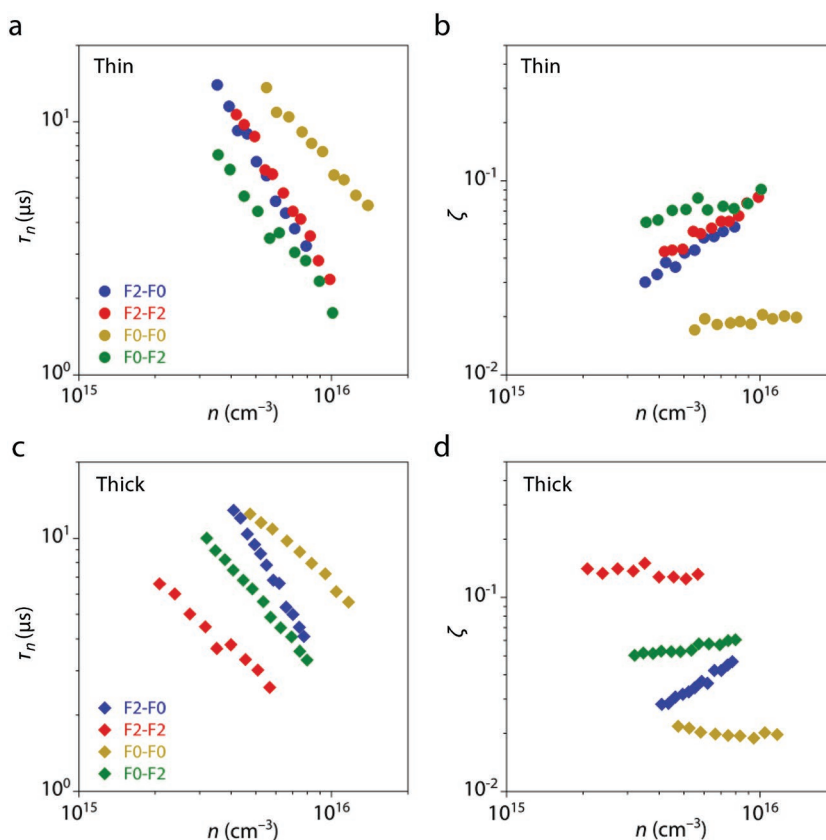

Figure 5. TPV and TPC analyses of polymer/PC$_{71}$BM cells with a,b) thin or c,d) thick active layers: a,c) charge carrier lifetime (τ_n) as a function of charge carrier density n and b,d) bimolecular recombination reduction factor ($\zeta = k_{rec}/k_L$) as a function of n.

is suppressed in bulk heterojunction OPVs.[70] Here, k_L is given by $k_L = e\mu/\varepsilon_0\varepsilon_r$, where μ is the slower charge carrier mobility,[71] ε_0 is the vacuum permittivity, and ε_r is the relative dielectric constant, which was assumed to be 3.5. Note that the SCLC-based charge carrier mobilities for the blend films as described above were used. Figure 5b displays the dependence of ζ on n for the thin devices. In all cases, ζ was evaluated to be on the order of 10^{-2}, which indicates that bimolecular recombination was substantially suppressed.

Figure 5c,d displays the results for the thick devices. ζ was evaluated to be on the order of 10^{-2} for **F0–F0**, **F2–F0**, and **F0–F2**, and to be on the order of 10^{-1} for **F2–F2**. This indicates that bimolecular recombination was still suppressed in the **F2–F0**-, **F0–F0**-, and **F0–F2**-based devices, but was enhanced in the **F2–F2**-based device and was close to the Langevin recombination when the active layer was thickened. More interestingly, ζ was larger in the **F2–F2**- and **F0–F2**-based devices than in the **F2–F0**- and **F0–F0**-based devices, which means that bimolecular recombination can be enhanced more significantly when the fluorine atoms were introduced on the bithiophene moiety. This trend correlates well with the fact that **F2–F2** and **F0–F2** had lower degree of polymer crystallinity particularly in the thick film than **F2–F0** and **F0–F0**, as revealed by the GIXD studies.

**ADVANCED
SCIENCE NEWS**

www.advancedsciencenews.com

**ADVANCED
ENERGY
MATERIALS**

www.advenergymat.de

8. Diode Characteristics of Cells

It has been known that FF and V_{oc} are closely related. In this section, we study the diode parameters of the cells by the dark J–V characteristics, and discuss the relationship between FF and V_{oc} and diode parameters by using the following empirical equations[72]

$$FF_0 = \frac{v_{OC} - \ln(v_{OC} + 0.72)}{v_{OC} + 1} \tag{1}$$

$$FF_s = FF_0(1 - 1.1r_s) + \frac{r_s^2}{5.4} \tag{2}$$

$$FF_{calc} = FF_s\left(1 - \frac{v_{OC} + 0.7}{v_{OC}}\frac{FF_s}{r_{sh}}\right) \tag{3}$$

Here, FF_0 is the fill factor of ideal solar cells with negligibly small series and shunt resistances, FF_s is the fill factor in consideration of only series resistance, and FF_{calc} is the fill factor in consideration of both series and shunt resistances. v_{OC} is the normalized open-circuit voltage expressed by $eV_{OC}/n_{id}k_BT$, where n_{id} is the ideality factor. r_s and r_{sh} are the normalized resistances expressed by R_sJ_{SC}/V_{OC} and $R_{sh}J_{SC}/V_{OC}$, respectively, where R_s and R_{sh} are actual series and shunt resistances, respectively. n_{id} can be evaluated by intensity-dependent J–V measurements, and R_s and R_{sh} can be evaluated by dark current analysis (Figures S14–S16, Supporting Information). Table S4 (Supporting Information) summarizes the diode parameters and experimental FF (FF_{exp}) and FF_{calc} of the cells. Although FF_{calc} values were higher than FF_{exp} values because the loss processes of photogenerated charges were not taken into account, these would be a good measure of the upper limit of FF. For thin cells, the FF_{calc} values of **F2–F0**- (0.79) and **F0–F0**-based cells (0.80) were lower than those of **F2–F0**- (0.82) and **F0–F2**-based cells (0.83). This is ascribed mainly to the lower V_{OC}, because n_{id} and R_s of the devices are comparable and R_{sh} is sufficiently large. For thick devices, however, the difference between FF_{calc} values (0.78 for **F2–F0**, 0.79 for **F2–F2** and **F0–F2**, and 0.80 for **F0–F2**) became smaller probably due to the larger R_s originating from the thick active layer.

9. Discussion on Thickness Dependence of FF

As we have shown above, the thickness dependence of FF was different between the polymers with the unsubstituted bithiophene moiety and the difluorinated bithiophene moiety: the latter showed more significant decrease in FF than the former by increasing thickness of the cell. We here discuss the correlation between FF and polymer order as well as charge recombination.

For the thin devices, FF was the highest for the **F0–F0** cell (0.75). For the other cells, the FF values of the **F2–F0** cell (0.68) and the **F0–F2** cell (0.69) were lower than that of the **F2–F2** cell (0.72) (Figure 3). The highest FF for the **F0–F0** cell would be explained by the favorable orientation and the high crystallinity of the polymer in the blend film and the substantially suppressed bimolecular recombination. On the other hand, it is

interesting that the **F2–F0** cell exhibited a low FF in spite of the favorable orientation and the high crystallinity of **F2–F0**, both of which were apparently similar to **F0–F0**. Although the SCLC-based hole mobility in the blend film was lower for **F2–F0** than for **F0–F0**, the difference was not significant when compared with other polymers as discussed above. The low FF in **F2–F0**-based cell compared to the **F0–F0** cell would rather be ascribed to the increased bimolecular recombination as proven by the larger ζ, although the origin is yet unclear. It is possible that the relatively low molecular weight of **F2–F0** compared to **F0–F0** might be the origin for the increase bimolecular recombination.

In addition, FF in the **F2–F0** cell was even lower than the **F2–F2** and **F0–F2** cells, despite the fact that **F2–F0** had desirable backbone orientation and high crystallinity as well as reduced bimolecular recombination compared to **F2–F2** and **F0–F2**. This could, in part, be ascribed to the relatively low V_{OC} for the **F2–F0** cell compared to the **F2–F2** and **F0–F2** cells. According to the empirical equation (see Equation (3) in the above section), a lower V_{OC} leads to a lower FF (FF_{calc}) particularly in a thinner cell. In fact, the calculated FF using the diode characteristics of the cells for the **F2–F0** cell was lower than that for the **F2–F2** and **F0–F2** cells by 0.03–0.04 (Table S4, Supporting Information), which is in good agreement with the difference in the experimental FF.

The lower FF for the **F0–F2** and **F2–F2** cells than for the **F0–F0** cell would be due to the relatively unfavorable orientation, as evidenced by the small fraction of the face-on orientation, and the relatively large ζ. The low FF for the **F0–F2** cell compared to the **F2–F2** cell should be attributed to the smaller fraction of the face-on orientation in **F0–F2**.

With increasing thickness of the active layer, FF decreased very gently for the **F0–F0**- and **F2–F0**-based cells, whereas FF decreased steeply for the **F2–F2**- and **F0–F2**-based cells. This is clearly explained by the difference in polymer order: the face-on fraction and crystallinity for **F2–F0** and **F0–F0** were much larger than those for **F2–F2** and **F0–F2** in the thick film. Further, bimolecular recombination was more suppressed in the **F2–F0** and **F0–F0** cells. For **F2–F2** and **F0–F2**, such an unfavorable polymer order as well as the large ζ would result in the low FF of the cell with a thick active layer. Note that the FF_{calc} values of the thick devices were almost the same, and thus this effect would be negligible. Thus, in the present polymer system, fluorination on the NTz moiety do not affect much on FF, whereas fluorination on the bithiophene moiety reduces FF particularly for the thick film, which is well-correlated with the polymer order as well as the bimolecular recombination.

10. Conclusions

We have synthesized new semiconducting polymers that incorporate difluoronaphthobisthiadiazole (FNTz), **F2–F0** and **F2–F2**, and discussed the influence of the substitution position of the fluorine atoms in the NTz and quaterthiophene copolymer system. The fluorination on the NTz moiety mainly deepened the LUMO energy level of the polymer, whereas the fluorination on the bithiophene moiety mainly deepened the HOMO energy level, which could be understood from the geometry of the LUMOs and HOMOs. Overall, the polymers with FNTz

(**F2–F0** and **F2–F2**) had narrower optical bandgaps than their NTz counterparts (**F0–F0** and **F0–F2**). The fluorination gave rise to the intramolecular locking of the polymer backbone by the noncovalent F···S interactions between the fluorine atom and the sulfur atom in the thiophene ring. However, the intramolecular locking was found to be stronger when the fluorine atoms were introduced on the bithiophene moiety rather than when they were introduced on the NTz moiety, which was likely due to the fact that the bithiophene moiety was locked with two F···S interactions whereas the NTz moiety had only one F···S interaction with the neighboring alkylthiophene moiety.

The photovoltaic performance of the polymers was studied by fabricating solar cells that used polymer/$PC_{71}BM$ films as the active layer. With the increased V_{OC} and thus the reduced E_{loss}, the **F2–F2** cell exhibited the highest power conversion efficiency of 10.8% among these polymers, which is one of the highest values reported so far for polymer/fullerene solar cells. Notably, the value was far higher than that of **F0–F4** having the same four fluorine atoms on the same polymer backbone but at different positions. However, it is interesting to note that the cell that used **F2–F2**, similarly to **F0–F2**, showed lower J_{SC} and FF than the cells that used **F2–F0** and **F0–F0** in particular when thick active layers were employed. The thickness dependence of FF was explained by the polymer order and the bimolecular recombination reduction factor, along with the empirical equation of FF. First, although **F2–F2** and **F0–F2** should have more coplanar backbones, the polymer crystallinity in the blend film was lower than that in the other films, particularly for the thick film. Then, these polymers had less favorable backbone orientation, in which the face-on fraction was smaller. Such polymer order in these polymers apparently led to the larger bimolecular recombination, resulting in the lower FF in the thick cells.

Although it has been shown in various semiconducting polymer systems that fluorination can effectively improve polymer electronic properties as well as polymer order, these results clearly show that the fluorination position must be carefully considered. Therefore, we believe that although the newly synthesized polymer, **F2–F2**, exhibited improved performance, careful molecular design would lead to new related polymers with even higher photovoltaic performance.

Supporting Information

Supporting Information is available from the Wiley Online Library or from the author.

[1] S. Günes, H. Neugebauer, N. S. Sariciftci, *Chem. Rev.* **2007**, *107*, 1324.

[2] J. R. Reynolds, B. C. Thompson, T. A. Skotheim, *Handbook of Conducting Polymers*, 4th ed. CRC Press, Boca Raton, FL **2007**.

[3] M. Leclerc, J.-F. Morin, *Design and Synthesis of Conjugated Polymers*, Wiley-VCH, Weinheim **2010**.

[4] C. Brabec, U. Scherf, V. Doyakonov, *Organic Photovoltaics: Materials, Device Physics, and Manufacturing Technologies*, Wiley-VCH, Weinheim **2008**.

[5] Y. Liang, Z. Xu, J. Xia, S.-T. Tsai, Y. Wu, G. Li, C. Ray, L. Yu, *Adv. Mater.* **2010**, *22*, E135.

[6] Z. He, C. Zhong, S. Su, M. Xu, H. Wu, Y. Cao, *Nat. Photonics* **2012**, *6*, 591.

[7] Y. Liu, J. Zhao, Z. Li, C. Mu, W. Ma, H. Hu, K. Jiang, H. Lin, H. Ade, H. Yan, *Nat. Commun.* **2014**, *5*, 5293.

[8] Y. Lin, J. Wang, Z.-G. Zhang, H. Bai, Y. Li, D. Zhu, X. Zhan, *Adv. Mater.* **2015**, *27*, 1170.

[9] V. Vohra, K. Kawashima, T. Kakara, T. Koganezawa, I. Osaka, K. Takimiya, H. Murata, *Nat. Photonics* **2015**, *9*, 403.

[10] J. Zhao, Y. Li, G. Yang, K. Jiang, H. Lin, H. Ade, W. Ma, H. Yan, *Nat. Energy* **2016**, *1*, 15027.

[11] W. Zhao, S. Li, H. Yao, S. Zhang, Y. Zhang, B. Yang, J. Hou, *J. Am. Chem. Soc.* **2017**, *139*, 7148.

[12] J. Yuan, Y. Zhang, L. Zhou, G. Zhang, H.-L. Yip, T.-K. Lau, X. Lu, C. Zhu, H. Peng, P. A. Johnson, M. Leclerc, Y. Cao, J. Ulanski, Y. Li, Y. Zou, *Joule* **2019**, *3*, 1140.

[13] D. Mühlbacher, M. Scharber, M. Morana, Z. Zhu, D. Waller, R. Gaudiana, C. Brabec, *Adv. Mater.* **2006**, *18*, 2884.

[14] J. Peet, J. Y. Kim, N. E. Coates, W. L. Ma, D. Moses, A. J. Heeger, G. C. Bazan, *Nat. Mater.* **2007**, *6*, 497.

[15] I. Osaka, G. Sauvé, R. Zhang, T. Kowalewski, R. D. McCullough, *Adv. Mater.* **2007**, *19*, 4160.

[16] L. Bürgi, M. Turbiez, R. Pfeiffer, F. Bienewald, H.-J. Kirner, C. Winnewisser, *Adv. Mater.* **2008**, *20*, 2217.

[17] Y. Zou, A. Najari, P. Berrouard, S. Beaupré, B. Réda Aïch, Y. Tao, M. Leclerc, *J. Am. Chem. Soc.* **2010**, *132*, 5330.

[18] R. Stalder, J. Mei, J. R. Reynolds, *Macromolecules* **2010**, *43*, 8348.

[19] Z. G. Zhang, J. Wang, *J. Mater. Chem.* **2012**, *22*, 4178.

[20] I. Osaka, M. Shimawaki, H. Mori, I. Doi, E. Miyazaki, T. Koganezawa, K. Takimiya, *J. Am. Chem. Soc.* **2012**, *134*, 3498.

[21] K. Kawashima, Y. Tamai, H. Ohkita, I. Osaka, K. Takimiya, *Nat. Commun.* **2015**, *6*, 10085.

**ADVANCED
SCIENCE NEWS**
www.advancedsciencenews.com

**ADVANCED
ENERGY
MATERIALS**
www.advenergymat.de

[22] T. Marszalek, M. Li, W. Pisula, *Chem. Commun.* **2016**, *52*, 10938.

[23] D. Baran, R. S. Ashraf, D. A. Hanifi, M. Abdelsamie, N. Gasparini, J. A. Röhr, S. Holliday, A. Wadsworth, S. Lockett, M. Neophytou, C. J. M. Emmott, J. Nelson, C. J. Brabec, A. Amassian, A. Salleo, T. Kirchartz, J. R. Durrant, I. McCulloch, *Nat. Mater.* **2017**, *16*, 363.

[24] J. Hou, O. Inganäs, R. H. Friend, F. Gao, *Nat. Mater.* **2018**, *17*, 119.

[25] H. Li, Z. Xiao, L. Ding, J. Wang, *Sci. Bull.* **2018**, *63*, 340.

[26] G. Zhang, J. Zhao, P. C. Y. Chow, K. Jiang, J. Zhang, Z. Zhu, J. Zhang, F. Huang, H. Yan, *Chem. Rev.* **2018**, *118*, 3447.

[27] X. Zhan, Z. Tan, B. Domercq, Z. An, X. Zhang, S. Barlow, Y. Li, D. Zhu, B. Kippelen, S. R. Marder, *J. Am. Chem. Soc.* **2007**, *129*, 7246.

[28] H. Yan, Z. Chen, Y. Zheng, C. Newman, J. R. Quinn, F. Dötz, M. Kastler, A. Facchetti, *Nature* **2009**, *457*, 679.

[29] C. Dou, X. Long, Z. Ding, Z. Xie, J. Liu, L. Wang, *Angew. Chem., Int. Ed.* **2016**, *55*, 1436.

[30] E. Zhou, J. Cong, Q. Wei, K. Tajima, C. Yang, K. Hashimoto, *Angew. Chem., Int. Ed.* **2011**, *50*, 2799.

[31] L. Zhu, W. Zhong, C. Qiu, B. Lyu, Z. Zhou, M. Zhang, J. Song, J. Xu, J. Wang, J. Ali, W. Feng, Z. Shi, X. Gu, L. Ying, Y. Zhang, F. Liu, *Adv. Mater.* **2019**, *31*, 1902899.

[32] M. Saito, I. Osaka, Y. Suda, H. Yoshida, K. Takimiya, *Adv. Mater.* **2016**, *28*, 6921.

[33] Y. Wang, Z. Yan, H. Guo, M. A. Uddin, S. Ling, X. Zhou, H. Su, J. Dai, H. Y. Woo, X. Guo, *Angew. Chem., Int. Ed.* **2017**, *56*, 15304.

[34] H. Sun, Y. Tang, C. W. Koh, S. Ling, R. Wang, K. Yang, J. Yu, Y. Shi, Y. Wang, H. Y. Woo, X. Guo, *Adv. Mater.* **2019**, *31*, 1807220.

[35] Y. Teshima, M. Saito, T. Fukuhara, T. Mikie, K. Komeyama, H. Yoshida, H. Ohkita, I. Osaka, *ACS Appl. Mater. Interfaces* **2019**, *11*, 23410.

[36] B. C. Thompson, J. M. J. Fréchet, *Angew. Chem., Int. Ed.* **2008**, *47*, 58.

[37] D. Veldman, S. C. J. Meskers, R. A. J. Janssen, *Adv. Funct. Mater.* **2009**, *19*, 1939.

[38] M. Wang, H. Wang, T. Yokoyama, X. Liu, Y. Huang, Y. Zhang, T.-Q. Nguyen, S. Aramaki, G. C. Bazan, *J. Am. Chem. Soc.* **2014**, *136*, 12576.

[39] W. Li, K. H. Hendriks, A. Furlan, M. M. Wienk, R. A. J. Janssen, *J. Am. Chem. Soc.* **2015**, *137*, 2231.

[40] I. Osaka, K. Takimiya, *Polymer* **2015**, *59*, A1.

[41] C. Piliego, T. W. Holcombe, J. D. Douglas, C. H. Woo, P. M. Beaujuge, J. M. J. Fréchet, *J. Am. Chem. Soc.* **2010**, *132*, 7595.

[42] A. T. Yiu, P. M. Beaujuge, O. P. Lee, C. H. Woo, M. F. Toney, J. M. J. Fréchet, *J. Am. Chem. Soc.* **2012**, *134*, 2180.

[43] L. Yang, J. R. Tumbleston, H. Zhou, H. Ade, W. You, *Energy Environ. Sci.* **2013**, *6*, 316.

[44] I. Osaka, M. Saito, T. Koganezawa, K. Takimiya, *Adv. Mater.* **2014**, *26*, 331.

[45] M. Saito, T. Koganezawa, I. Osaka, *ACS Appl. Mater. Interfaces* **2018**, *10*, 32420.

[46] H. Huang, L. Yang, A. Facchetti, T. J. Marks, *Chem. Rev.* **2017**, *117*, 10291.

[47] Z. Fei, M. Shahid, N. Yaacobi-Gross, S. Rossbauer, H. Zhong, S. E. Watkins, T. D. Anthopoulos, M. Heeney, *Chem. Commun.* **2012**, *48*, 11130.

[48] H. Bronstein, J. M. Frost, A. Hadipour, Y. Kim, C. B. Nielsen, R. S. Ashraf, B. P. Rand, S. Watkins, I. McCulloch, *Chem. Mater.* **2013**, *25*, 277.

[49] Z. Fei, P. Boufflet, S. Wood, J. Wade, J. Moriarty, E. Gann, E. L. Ratcliff, C. R. McNeill, H. Sirringhaus, J.-S. Kim, M. Heeney, *J. Am. Chem. Soc.* **2015**, *137*, 6866.

[50] K. Kawashima, T. Fukuhara, Y. Suda, Y. Suzuki, T. Koganezawa, H. Yoshida, H. Ohkita, I. Osaka, K. Takimiya, *J. Am. Chem. Soc.* **2016**, *138*, 10265.

[51] M. Wang, X. Hu, P. Liu, W. Li, X. Gong, F. Huang, Y. Cao, *J. Am. Chem. Soc.* **2011**, *133*, 9638.

[52] Y. Jin, Z. Chen, S. Dong, N. Zheng, L. Ying, X.-F. Jiang, F. Liu, F. Huang, Y. Cao, *Adv. Mater.* **2016**, *28*, 9811.

[53] S. Chatterjee, Y. Ie, T. Seo, T. Moriyama, G.-J. A. H. Wetzelaer, P. W. M. Blom, Y. Aso, *NPG Asia Mater.* **2018**, *10*, 1016.

[54] J. C. Bijleveld, V. S. Gevaerts, D. D. Nuzzo, M. Turbiez, S. G. J. Mathijssen, D. M. de Leeuw, M. M. Wienk, R. A. J. Janssen, *Adv. Mater.* **2010**, *22*, E242.

[55] I. Osaka, T. Abe, M. Shimawaki, T. Koganezawa, K. Takimiya, *ACS Macro Lett.* **2012**, *1*, 437.

[56] J. R. Matthews, W. Niu, A. Tandia, A. L. Wallace, J. Hu, W.-Y. Lee, G. Giri, S. C. B. Mannsfeld, Y. Xie, S. Cai, H. H. Fong, Z. Bao, M. He, *Chem. Mater.* **2013**, *25*, 782.

[57] H. Yoshida, *Chem. Phys. Lett.* **2012**, *539–540*, 180.

[58] H. Yoshida, *J. Electron Spectrosc. Relat. Phenom.* **2015**, *204*, 116.

[59] K. Yamada, S. Yanagisawa, T. Koganezawa, K. Mase, N. Sato, H. Yoshida, *Phys. Rev. B* **2018**, *97*, 245206.

[60] F. Wang, K. Nakano, H. Yoshida, K. Hashimoto, H. Segawa, C.-S. Hsu, K. Tajima, *J. Mater. Chem. A* **2018**, *6*, 22889.

[61] J. Rivnay, S. C. B. Mannsfeld, C. E. Miller, A. Salleo, M. F. Toney, *Chem. Rev.* **2012**, *112*, 5488.

[62] D. T. Duong, M. F. Toney, A. Salleo, *Phys. Rev. B* **2012**, *86*, 205205.

[63] M. Saito, T. Koganezawa, I. Osaka, *ACS Appl. Polym. Mater.* **2019**, *1*, 1257.

[64] J. T. Rogers, K. Schmidt, M. F. Toney, E. J. Kramer, G. C. Bazan, *Adv. Mater.* **2011**, *23*, 2284.

[65] R.-J. Roe, *Methods of X-Ray and Neutron Scattering in Polymer Science*, Oxford University Press, Oxford **2010**.

[66] C. B. Nielsen, A. J. P. White, I. McCulloch, *J. Org. Chem.* **2015**, *80*, 5045.

[67] J. A. Bartelt, D. Lam, T. M. Burke, S. M. Sweetnam, M. D. McGehee, *Adv. Energy Mater.* **2015**, *5*, 1500577.

[68] A. Maurano, C. G. Shuttle, R. Hamilton, A. M. Ballantyne, J. Nelson, W. Zhang, M. Heeney, J. R. Durrant, *J. Phys. Chem. C* **2011**, *115*, 5947.

[69] D. Credgington, J. R. Durrant, *J. Phys. Chem. Lett.* **2012**, *3*, 1465.

[70] C. Göhler, A. Wagenpfahl, C. Deibel, *Adv. Electron. Mater.* **2018**, *4*, 1700505.

[71] L. J. A. Koster, V. D. Mihailetchi, P. W. M. Blom, *Appl. Phys. Lett.* **2006**, *88*, 052104.

[72] B. Qi, J. Wang, *Phys. Chem. Chem. Phys.* **2013**, *15*, 8972.